Highly insulating thermoplastic nanocomposites based on a polyolefin ternary blend for high-voltage direct current power cables

Nanoscale

PAPER

View Article Online
View Journal

Cite this: DOI: 10.1039/d1nr08255h

Highly insulating thermoplastic nanocomposites based on a polyolefin ternary blend for high-voltage direct current power cables†

Azadeh Soroudi,[a] Yingwei Ouyang,[a] Fritjof Nilsson,[b,c] Ida Östergren,[a] Xiangdong Xu,[d] Zerui Li,[a] Amir Masoud Pourrahimi,[a] Mikael Hedenqvist,[b] Thomas Gkourmpis,[e] Per-Ola Hagstrand[e] and Christian Müller *[a]

Octyl-silane-coated Al_2O_3 nanoparticles are found to be a promising conductivity-reducing additive for thermoplastic ternary blends comprising low-density polyethylene (LDPE), isotactic polypropylene and a styrenic copolymer. The ternary blend nanocomposites were prepared by compounding the blend components together with an LDPE-based masterbatch that contained the nanoparticles. The nanoparticles did not affect the superior stiffness of the ternary blends, compared to neat LDPE, between the melting temperatures of the two polyolefins. As a result, ternary blend nanocomposites comprising 38 wt% polypropylene displayed a storage modulus of more than 10 MPa up to at least 150 °C, independent of the chosen processing conditions. Moreover, the ternary blend nanocomposites featured a low direct-current electrical conductivity of about 3×10^{-15} S m^{-1} at 70 °C and an electric field of 30 kV mm^{-1}, which could only be achieved through the presence of both polypropylene and Al_2O_3 nanoparticles. This synergistic conductivity-reducing effect may facilitate the design of more resistive thermoplastic insulation materials for high-voltage direct current (HVDC) power cables.

Received 15th December 2021,
Accepted 11th May 2022

DOI: 10.1039/d1nr08255h

rsc.li/nanoscale

Introduction

High-voltage direct current (HVDC) power cables are an important component of future power grids that seamlessly integrate renewable sources of energy. The most common type of extruded HVDC cables comprise a polymeric insulation layer composed of crosslinked polyethylene (XLPE). The XLPE insulation layer is obtained by peroxide curing of low-density polyethylene (LDPE), which has a melting temperature of $T_m^{LDPE} \approx 110$ °C. Peroxide curing requires a degassing step to remove volatile by-products that arise from the crosslinking reaction.[1] Alternative insulation materials that do not require degassing, such as polymer blends crosslinked *via* a click-chemistry type curing reaction[2] and thermoplastic materials based on, *e.g.*, blends or copolymers comprising polypropylene (PP),[3–5] receive considerable attention. The high melting temperature of PP materials, which can be as high as $T_m^{PP} \approx 170$ °C, alleviates the need for crosslinking.[6–8] In addition, materials with a higher melting temperature may allow the design of HVDC cables that could endure higher operating temperatures than the 70 to 90 °C, which are common for HVDC cables.[6,9]

Significant academic research efforts are currently dedicated to the development of materials concepts that permit to reduce the direct-current (DC) electrical conductivity σ_{DC} of insulation materials at high electric fields. A reduction in σ_{DC} may allow the design of HVDC cables that can operate at a higher transmission voltage and hence incur lower losses. LDPE and XLPE feature values of $\sigma_{DC} \geq 10^{-14}$ S m^{-1} at 30 kV mm^{-1} and 70 °C,[10] which are common design parameters for the highest electric field stress and operating temperature that the insulation layer of an HVDC cable may experience.[8] Conductivity-reducing additives such as metal oxide nanoparticles,[11] organic semiconductors including fullerenes[12] and conjugated polymers,[13] aromatic voltage stabilizers,[14–16] as well as high-density polyethylene (HDPE)[10] can be added to the polyethylene-based insulation material to achieve a further reduction in σ_{DC}. Moreover, the combination of different additives such as Al_2O_3 nanoparticles and HDPE can give rise to a synergistic conductivity-reducing effect.[17]

PP grades developed for capacitor type applications display excellent electrical properties[18] and an electrical conductivity

[a]Department of Chemistry and Chemical Engineering, Chalmers University of Technology, 41296 Göteborg, Sweden
[b]Department of Fibre and Polymer Technology, School of Engineering Sciences in Chemistry, Biotechnology and Health, KTH Royal Institute of Technology, 10044 Stockholm, Sweden
[c]FSCN research centre, Mid Sweden University, 85170 Sundsvall, Sweden
[d]Department of Electrical Engineering, Chalmers University of Technology, 41296 Göteborg, Sweden
[e]Innovation & Technology, Borealis AB, 44486 Stenungsund, Sweden.
E-mail: christian.muller@chalmers.se

† Electronic supplementary information (ESI) available. See DOI: https://doi.org/10.1039/d1nr08255h

as low as $\sigma_{DC} \approx 10^{-15}$ S m^{-1} at 30 kV mm^{-1} and 70 °C has been reported for isotactic PP.[3] A number of studies have recently investigated nanocomposites of polyolefin-based insulation materials and metal oxide nanoparticles composed of MgO,[19–21] ZnO,[21–23] TiO_2,[21,24] SiO_2[25,26] or Al_2O_3.[21,27,28] The strongest conductivity-reducing effect is typically observed if the metal oxide nanoparticles are surface-modified with, *e.g.*, silane coupling agents terminated with an alkyl chain.[19,29]

We have recently explored blends of PP and LDPE to which we added a linear triblock copolymer, polystyrene-*b*-(ethylene-*co*-butylene)-*b*-polystyrene (SEBS),[3] which modifies the interface between domains of the two immiscible polyolefins. Ternary blends with a sufficiently high content of both PP and SEBS displayed a high storage modulus of more than 10 MPa at temperatures up to T_m^{PP}, which may allow the design of insulation materials with higher operating temperatures. Moreover, the addition of PP to LDPE considerably reduced the electrical conductivity.[30]

Here, we show that the addition of Al_2O_3 nanoparticles surface-modified with *n*-octyltriethoxysilane allows to further reduce the electrical conductivity of SEBS : PP : LDPE ternary blends without affecting the high-temperature dimensional stability. Al_2O_3 nanoparticles are a commonly used additive for plastics because they are fairly inert, odourless, inexpensive and white. Furthermore, they can be surface-functionalized for good dispersion in molten LDPE and for improving its insulating properties.[17,31] The presence of both Al_2O_3 nanoparticles and PP has a synergistic conductivity-reducing effect, reaching an electrical conductivity close to neat PP, which may aid the design of highly insulating materials.

Experimental

Materials

LDPE with a melt flow index MFI ≈ 2 g per 10 min (190 °C/2.16 kg), number-average molecular weight $M_n \approx 13$ kg mol^{-1}, polydispersity index PDI ≈ 9 and number of long-chain branches ≈ 1.9 as well as PP with an $M_n \approx 40$ kg mol^{-1}, PDI ≈ 9 and isotacticity > 90% were obtained from Borealis AB. Polystyrene-*b*-(ethylene-co-butylene)-*b*-polystyrene (SEBS) with an MFI < 1 g per 10 min (230 °C per 2.16 kg) and a polystyrene content of 18.5–22.5% was obtained from Kraton Corporation (Kraton G1642 HU). Al_2O_3 nanoparticles (Nanodur; density ρ = 3.97 g cm^{-3}) were obtained from Nanophase Inc. *N*-Octyltriethoxysilane and the antioxidant Irganox 1076 were obtained from Sigma-Aldrich and Ciba Speciality Chemicals, respectively.

Sample preparation

Al_2O_3 nanoparticles with an average diameter of (50 ± 25) nm were surface-modified with *n*-octyltriethoxysilane according to a previously described procedure.[17] After surface modification, the nanoparticles were dried for 20 h at 80 °C in a vacuum oven and then dispersed in n-heptane (0.3 ml *n*-heptane per 1 g polymer) through ultrasonication for 5 minutes, followed by the addition of Irganox 1076 and LDPE, resulting in a solid content of 3 wt% Al_2O_3 nanoparticles, 97 wt% LDPE and 0.02 wt% Irganox 1076. The LDPE : nanoparticle slurry was shaken for 1 h and dried overnight at 80 °C. The dried powder was shaken for another 30 min and then compounded for 6 min at 150 °C and 100 rpm with a MC15 twin-screw microcompounder from Xplore. The LDPE : Al_2O_3 extrudate was cut into 2–3 mm long granules. Neat LDPE, the LDPE nanocomposites, ternary blends and the ternary blend nanocomposites were prepared by compounding different amounts of SEBS, PP, LDPE and the LDPE : Al_2O_3 masterbatch (dried for 17 h at 80 °C in a vacuum oven) with a MC5 twin-screw microcompounder from Xplore under nitrogen gas for 4 min at 200 °C and 70 rpm followed by extrusion using a die temperature of 210 °C. Extrudates were compression molded into 0.3 mm thick films for electrical measurements and 1.9 mm thick films for mechanical analysis using a LabPro 200 Fontijne press at 200 °C by applying a pressure of 3800 kPa for 1 min followed by cooling at a rate of −10 °C min^{-1}, unless indicated otherwise. PP and SEBS pellets were used as received and compression molded at the same conditions. To prepare XLPE, milled LDPE was dispersed in a solution of dicumyl peroxide (DCP) in methanol at 40 °C and stirred for 1 h, followed by solvent evaporation. The resulting milled LDPE infused with 1 wt% DCP was compression molded at 120 °C for 5 min, followed by annealing at 180 °C for 10 min to facilitate crosslinking. The resulting XLPE had a gel content of 72%, determined according to a previously described procedure.[32]

Scanning electron microscopy (SEM)

Samples for SEM were cryofractured and subsequently etched for 45 min using a solution of 1 wt% potassium permanganate in a mixture of sulfuric acid, *ortho*-phosphoric acid, and water, followed by cleaning in hydrogen peroxide, water and methanol. The etched surfaces were sputtered with palladium and imaged with a LEO Ultra 55 SEM instrument, using an acceleration voltage of 3 kV.

Differential scanning calorimetry (DSC)

DSC measurements were carried out under nitrogen between −25 and 200 °C at a scan rate of 10 °C min^{-1}, using a Mettler Toledo DSC2 calorimeter equipped with a HSS7 sensor and a TC-125MT intercooler. The sample weight was 4–8 mg.

Wide angle X-ray scattering (WAXS)

Transmission WAXS diffractograms were obtained under ambient atmosphere using a Mat:Nordic instrument from SAXSLAB equipped with a Rigaku 003+ high brilliance micro focus Cu-radiation source (wavelength = 1.5406 Å) and a Pilatus 300 K detector placed at a distance of 126 mm from the sample.

Dynamic mechanical analysis (DMA)

DMA was carried out using a TA Q800 DMA in tensile mode on 35 mm times 6 mm large pieces cut from 1.9 mm thick melt-pressed films. Variable-temperature measurements were done

at a heating rate of 3 °C min^{-1}, with a maximum strain of 0.05% and a frequency of 0.5 Hz.

DC conductivity measurements

The DC conductivity test cell consisted of a three-electrode system, a high voltage electrode, a guard ring electrode and a measuring electrode with Ø = 60 mm. Prior to the measurements, the samples were dried for 24 h at 70 °C in a vacuum oven together with the test cell. The high voltage electrode was connected to a high-voltage power supply (Glassman FJ60R2). A DC electric field of 30 kV mm^{-1} was applied across a 0.3 mm thick specimen for 19 h and its volume leakage current was recorded with a Keithley 6517B electrometer and a LabView based dynamic average software. σ_{DC} was calculated based on the leakage currents obtained after 18 h.

Results and discussion

We chose to work with a masterbatch of LDPE that contained 3 wt% of octyl-silane-coated Al_2O_3 nanoparticles with an average diameter of 50 nm, prepared according to a previously described procedure (see Experimental for details).[17] Nanocomposites were prepared by compounding the LDPE : Al_2O_3 masterbatch with either neat LDPE to prepare LDPE : Al_2O_3 nanocomposites or SEBS and PP to prepare SEBS : PP : LDPE : Al_2O_3 ternary blend nanocomposites (see Table 1 and Table S1† for compositions of the prepared formulations). The extrudates were cut and then compression molded into films at 200 °C (Fig. 1).[3] We chose to focus our study on ternary blend nanocomposites with a formulation of 20 : 38 : 40.7 : 1.3 SEBS : PP : LDPE : Al_2O_3 because we have previously observed that ternary blends with a comparable PP content display both excellent mechanical and electrical properties, which are not overly affected by changes in processing conditions.[30]

Scanning electron microscopy (SEM) on cryofractured, etched and sputtered surfaces was carried out to examine the microstructure of the nanocomposites. SEM images of a 98.7 : 1.3 LDPE : Al_2O_3 nanocomposite feature distinct Al_2O_3 nanoparticles embedded in the LDPE matrix (Fig. 2a; SEM images of the same LDPE grade can be found in ref. 10). The 20 : 38 : 42 SEBS : PP : LDPE ternary blend displayed a heterogeneous microstructure (Fig. 2b). The etching process that was employed predominately removes amorphous material, resulting in voids where the SEBS copolymer used to reside. Hence, we assign the regions that contain voids to SEBS, intermixed with PP, which are interspersed with domains of LDPE (Fig. 2b). The regions composed of PP and SEBS (voids in the SEM image shown in Fig. 2b) appear continuous, which is consistent with a previous study.[30] SEM images of the 20 : 38 : 40.7 : 1.3 SEBS : PP : LDPE : Al_2O_3 ternary blend nanocomposite feature a comparable microstructure with continuous PP : SEBS domains interspersed with LDPE domains (Fig. 2c). The Al_2O_3 nanoparticles were added *via* an LDPE : Al_2O_3 masterbatch and hence can be expected to predominately reside within LDPE domains, as confirmed by SEM images of the ternary blend nanocomposite (Fig. 2c). We also investigated LDPE-rich ternary blend nanocomposites with a formulation of 5 : 24 : 68.9 : 2.1 SEBS : PP : LDPE : Al_2O_3, which featured a microstructure composed of SEBS:PP droplets in a continuous LDPE matrix (Fig. S1†). Again, the Al_2O_3 nanoparticles were located within LDPE.

Differential scanning calorimetry (DSC) was carried out to explore whether some of the Al_2O_3 nanoparticles have entered

Table 1 Composition of the investigated formulations as well as their storage modulus E' and DC electrical conductivity σ_{DC} measured at 70 °C and 30 kV mm^{-1}

	LDPE (wt%)	PP (wt%)	SEBS (wt%)	Al_2O_3 (wt%)	E' at 150 °C (MPa)	σ_{DC} at 70 °C (10^{-15} S m^{-1})
LDPE	100	—	—	—	n.a.	43.0 ± 4.3[a]
LDPE : Al_2O_3	98.7	—	—	1.3	n.a.	9.6 ± 1.5[b]
PP	—	100	—	—	220	1.4 ± 0.1[c]
SEBS	—	—	100	—	2	10.1 ± 1.0[a]
SEBS : PP : LDPE	42	38	20	—	15	4.3 ± 0.4[a]
SEBS : PP : LDPE : Al_2O_3	40.7	38	20	1.3	19	2.6 ± 0.4[b]

[a] Single measurement, a relative error of Δx = 10% is assumed. [b] Mean of two measurements of two separately compounded samples, error calculated according to $\Delta x = (x_{max} - x_{min})/2$. [c] Data from ref. 30.

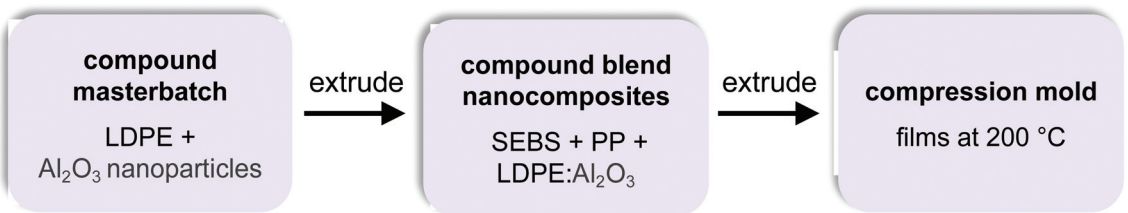

Fig. 1 Processing scheme used for the preparation of ternary blend nanocomposite films.

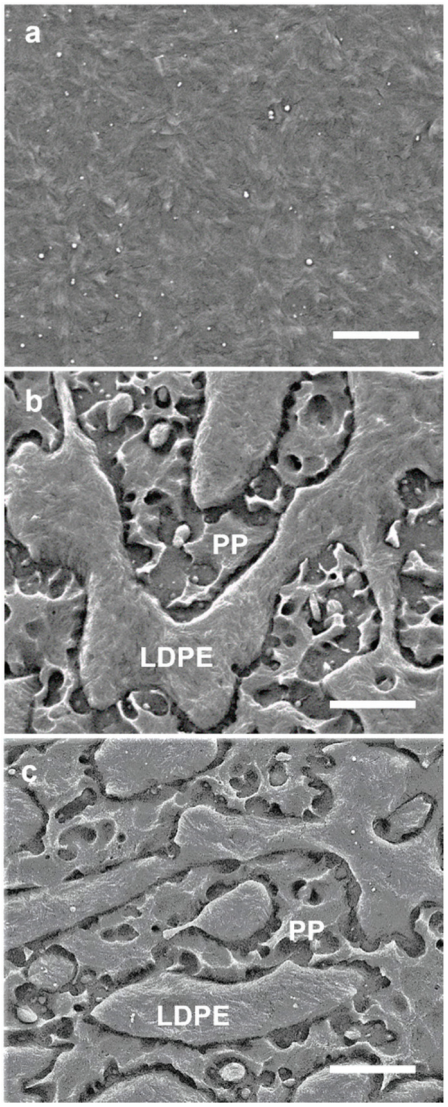

Fig. 2 SEM micrographs of the cryofractured, etched and sputtered surfaces of (a) the LDPE : Al_2O_3 nanocomposite, (b) the 20 : 38 : 42 SEBS : PP : LDPE ternary blend, and (c) the 20 : 38 : 40.7 : 1.3 SEBS : PP : LDPE : Al_2O_3 ternary blend nanocomposite (all scale bars correspond to 2 μm).

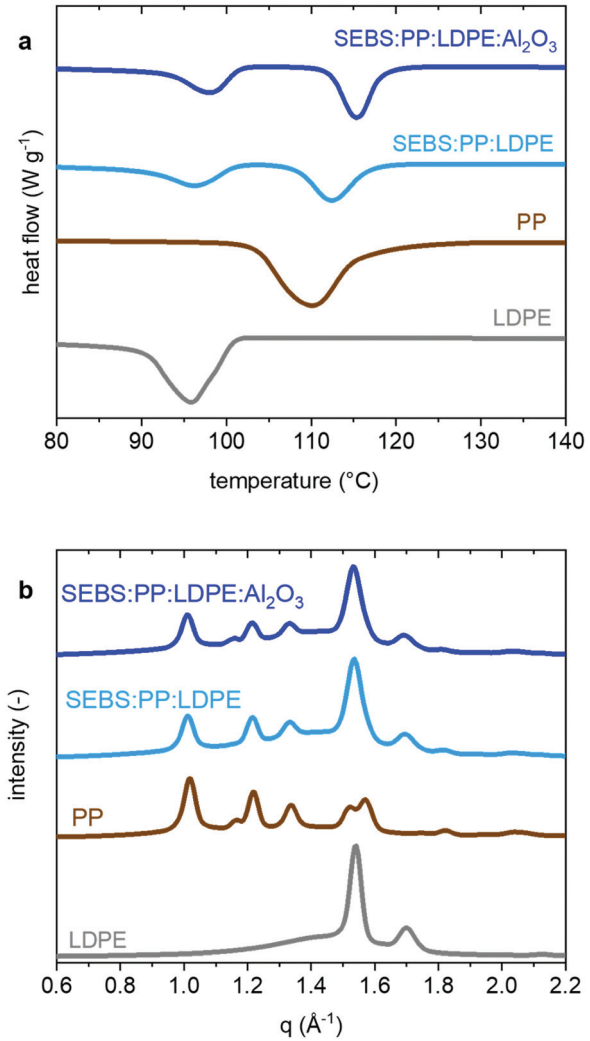

Fig. 3 (a) DSC cooling thermograms and (b) WAXS diffractograms of LDPE (grey), PP (brown), 20 : 38 : 42 SEBS : PP : LDPE (blue) and the 20 : 38 : 40.7 : 1.3 SEBS : PP : LDPE : Al_2O_3 nanocomposite (sky blue).

PP domains during compounding. A comparison of DSC cooling thermograms of the 20 : 38 : 42 SEBS : PP : LDPE ternary blend and 20 : 38 : 40.7 : 1.3 SEBS : PP : LDPE:Al_2O_3 ternary blend nanocomposite indicate that the peak crystallization temperature of PP shifts from $T_c^0 \approx 112$ °C to $T_c^{nuc} \approx 115$ °C, which we ascribe to the presence of Al_2O_3 nanoparticles that nucleate PP (Fig. 3a and Table S2†). Since the two materials feature a similar microstructure, we propose that some of the nanoparticles have entered PP domains (or reside at the PP domain interface) and act as a nucleating agent (note that T_c^{PE} also increased from 96 °C to 98 °C, which would again be consistent with a nucleation type effect). To investigate the ability of Al_2O_3 to nucleate PP in more detail we calculated the nucleating efficiency of Al_2O_3 with respect to optimally self-seeded material according to $\eta_{nuc} = (T_c^{nuc} - T_c^0)/(T_c^{max} - T_c^0)$ where T_c^{nuc}, T_c^0 and T_c^{max} are the peak crystallization temperatures of nucleated material, non-nucleated material and optimally nucleated material, respectively.[33] T_c^{max} can be obtained through self-seeding where the material is only allowed to melt in part, which yields $T_c^{max} \approx 141$ °C for PP in case of the 20 : 38 : 42 SEBS : PP : LDPE ternary blend (Fig. S2†). Hence, we obtain $\eta_{nuc} \approx 10\%$ for PP, which is low compared to nucleating agents such as dimethyldibenzylidene sorbitol (DMDBS).[34]

The crystallinity of PP and PE was not overly affected by the Al_2O_3 nanoparticles (Table S2†), in agreement with previous reports.[17,27] Wide angle X-ray scattering (WAXS) diffractograms of the ternary blend and ternary blend nanocomposite (Fig. 3b) indicate that in case of the ternary blend, only PP α-polymorph crystallites are present. Instead, the presence of Al_2O_3 nanoparticles promotes the formation of a fraction of β-polymorph crystallites as evidenced by the emergence of a

clear peak at q = 1.16 Å^{-1}, which is consistent with a nucleation type effect.[35]

In a further set of experiments, we used dynamic mechanical analysis (DMA) to record the storage modulus E' of the investigated materials as a function of temperature (Fig. 4). The DMA thermograms of neat LDPE and the 98.7 : 1.3 LDPE : Al_2O_3 nanocomposite show comparable behavior and a strong reduction in modulus above $T_m^{LDPE} \approx 110$ °C. Likewise, the DMA thermograms recorded for the 20 : 38 : 42 SEBS : PP : LDPE ternary blend and the corresponding nanocomposite follow a similar trend (Fig. 4), which is consistent with the comparable microstructure inferred from SEM (see Fig. 2) and similar crystallinity (Table S2†). Gratifyingly, both materials feature a relatively high modulus in the temperature range $T_m^{LDPE} < T < T_m^{PP}$, with a value of E' = 15 MPa at 150 °C above which PP starts to melt (Table 1). In this temperature range the storage modulus of the ternary blend is about two orders of magnitude higher than the rubber plateau value of XLPE, which is today widely used as an HVDC insulation material. Furthermore, we observed a comparable thermo-mechanical behaviour independent of the cooling rate used for sample preparation, ranging from −1 to −20 °C min^{-1} (Fig. S3†), which indicates that the here investigated formulations are not sensitive to slight changes in processing conditions.

We went on to investigate the impact of the octyl-silane-coated Al_2O_3 nanoparticles on the electrical conductivity (Fig. 5). For neat LDPE we measure a value of $\sigma_{DC} \approx 43 \times 10^{-15}$ S m^{-1} at 70 °C and 30 kV mm^{-1} (Table 1), which is in agreement with previous studies where we have investigated the same LDPE grade.[3,32] The presence of 1.3 wt% Al_2O_3 nanoparticles reduced the electrical conductivity to 9.6 × 10^{-15} S m^{-1}, which confirms that the here employed nanoparticles have a clear conductivity-reducing effect. The mechanism behind the reduced DC conductivity displayed by nanocomposites is not yet fully established. However, several hypotheses have been proposed. Dispersed nanoparticles in an LDPE matrix can absorb polar molecules or ions, which act as charge carriers,[36,37] they can introduce deep trapping sites for electrons or holes located in the vicinity of the nanoparticle surface[38–42] and they can lead to recombination of charge carriers.[43]

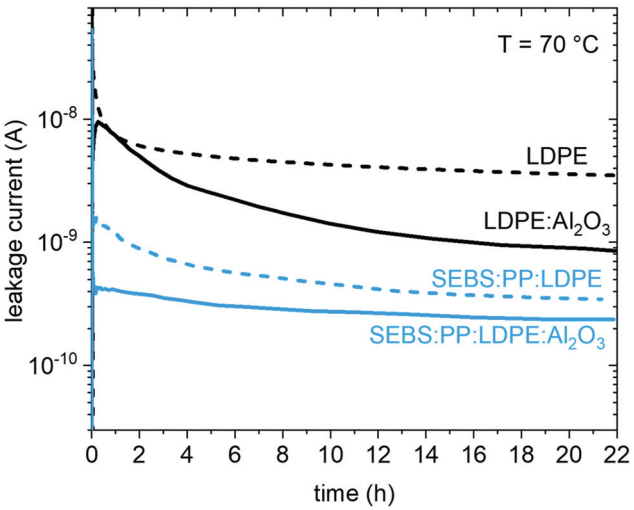

Fig. 5 Leakage current at 70 °C and 30 kV mm^{-1} as a function of time of neat LDPE (black-dash), 98.7 : 1.3 LDPE : Al_2O_3 (black-solid), 20 : 38 : 42 SEBS : PP : LDPE (blue-dash), and 20 : 38 : 40.7 : 1.3 SEBS : PP : LDPE : Al_2O_3 (blue-solid).

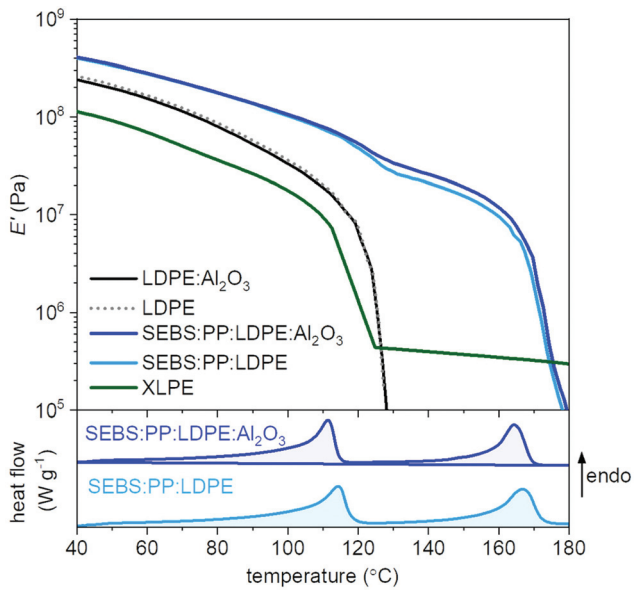

Fig. 4 Top: Storage modulus E' measured with DMA for LDPE (grey), 98.7 : 1.3 LDPE:Al_2O_3 (black), 20 : 38 : 42 SEBS : PP : LDPE (blue), 20 : 38 : 40.7 : 1.3 SEBS : PP : LDPE : Al_2O_3 (sky blue) and XLPE (olive); bottom: DSC heating thermograms of 20 : 38 : 42 SEBS : PP:LDPE (blue) and 20 : 38 : 40.7 : 1.3 SEBS : PP : LDPE : Al_2O_3 (sky blue).

The 20 : 38 : 42 SEBS : PP : LDPE ternary blend displayed a conductivity of $\sigma_{DC} \approx 4.3 \times 10^{-15}$ S m^{-1} at 70 °C and 30 kV mm^{-1}, which is 10-times lower than the value measured for neat LDPE (Table 1). We ascribe the strong reduction in σ_{DC} to the presence of PP, which thanks to its high degree of cleanliness has a conductivity of only $\sigma_{DC} \approx 1.4 \times 10^{-15}$ S m^{-1}. The addition of 1.3 wt% Al_2O_3 nanoparticles results in a further reduction in σ_{DC} to 2.6 × 10^{-15} S m^{-1} at 70 °C and 30 kV mm^{-1}, measured for the 20 : 38 : 40.7 : 1.3 SEBS : PP : LDPE : Al_2O_3 ternary blend nanocomposite. A similar trend is also observed at 50 °C, *i.e.* the addition of Al_2O_3 nanoparticles to the ternary blend results in a material that has a lower σ_{DC} than the ternary blend without Al_2O_3 (Fig. S4†). SEM images indicate that the SEBS : PP regions are continuous (see Fig. 2), and therefore it can be anticipated that charge conduction involves SEBS:PP regions. Al_2O_3 nanoparticles are present in LDPE domains (see Fig. 2c) as well as in PP domains, inferred from the nucleating effect observed with DSC (see Fig. 3). We argue that Al_2O_3 nanoparticles function as a conductivity-reducing additive also in case of the ternary blend nanocomposite.

In a last set of experiments, we measured σ_{DC} of a ternary blend with a composition of 5 : 24 : 71 SEBS : PP : LDPE, which features isolated SEBS:PP regions embedded in a continuous LDPE matrix (see Fig. S1†), as well as a corresponding binary blend with a composition of 25 : 75 PP : LDPE. For this LDPE-rich ternary blend we recorded a value of $\sigma_{DC} \approx 11.6 \times 10^{-15}$ S m^{-1}, which was reduced to 2.9×10^{-15} S m^{-1} in the case of the corresponding ternary blend nanocomposite containing 2.1 wt% of Al_2O_3 nanoparticles (Fig. S5 and Table S1†), again prepared by compounding the LDPE:Al_2O_3 masterbatch with SEBS and PP (see Fig. 1). We argue that also for the more LDPE-rich ternary blend nanocomposite, the Al_2O_3 nanoparticles function as a conductivity-reducing additive, resulting in a 4-fold reduction in σ_{DC}.

A comparison of the DC electrical conductivity measured for materials with different LDPE contents reveals that in case of formulations that do not contain any nanoparticles there is a gradual reduction in σ_{DC} with increasing amount of the foreign phase (PP or SEBS : PP) with the lowest value obtained for neat PP (Fig. 6). In contrast, the materials that contain Al_2O_3 nanoparticles display a much lower σ_{DC} of about 3×10^{-15} S m^{-1}, largely independent of the LDPE content. In case of LDPE-rich nanocomposite formulations, the reduction in σ_{DC} is more pronounced compared to corresponding formulations with a similar LDPE content but no Al_2O_3 nanoparticles. Evidently, the use of Al_2O_3 nanoparticles as a conductivity-reducing additive is a viable strategy for the design of highly resistive insulation materials, in particular in case of formulations that contain a large amount of LDPE.

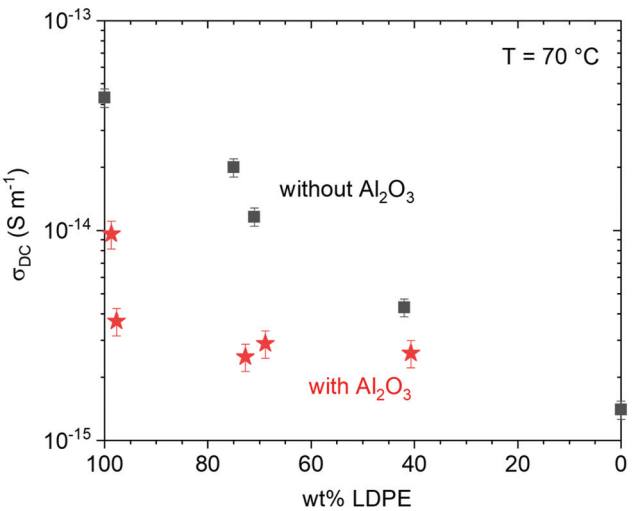

Fig. 6 DC electrical conductivity σ_{DC} at 70 °C and 30 kV mm^{-1} as a function of LDPE content in wt% (indicated in bold) of formulations without Al_2O_3 (black squares) including neat PP (**0**), neat LDPE (**100**), 25 : **75** PP:LDPE, 5 : 24 : **71** SEBS : PP : LDPE and 20 : 38 : **42** SEBS : PP : LDPE, as well as with Al_2O_3 (red stars) including **98.7** : 1.3 LDPE:Al_2O_3, **97.7** : 2.3 LDPE : Al_2O_3, 25 : **72.8** : 2.2 PP : LDPE : Al_2O_3, 5 : 24 : **68.9** : 2.1 SEBS : PP : LDPE : Al_2O_3 and 20 : 38 : **40.7** : 1.3 SEBS : PP : LDPE : Al_2O_3.

Conclusions

Octyl-silane-coated Al_2O_3 nanoparticles are a promising conductivity-reducing additive for SEBS : PP : LDPE ternary blends. The addition of Al_2O_3 nanoparticles through compounding of an LDPE : Al_2O_3 masterbatch with SEBS and PP does not alter the domain size and shape as compared to SEBS : PP : LDPE ternary blends with a comparable composition. As a result, the ternary blend nanocomposite, which features continuous SEBS : PP regions, displays a high storage modulus of more than 10 MPa between the melting temperatures of LDPE and PP. Some of the Al_2O_3 nanoparticles appear to enter the PP domains (or PP domain interface) during compounding, as evidenced by a nucleation type effect. Importantly, ternary blend nanocomposites feature a DC electrical conductivity as low as 2.6×10^{-15} S m^{-1} at 70 °C and 30 kV mm^{-1}, which for the investigated formulation can only be achieved through the simultaneous presence of highly insulating PP and Al_2O_3 nanoparticles. Further work should focus on an in-depth characterization of the dielectric properties, such as space charge accumulation and breakdown strength of the ternary blend nanocomposite, including thermally aged material. In addition, it is feasible that also other types of metal oxide nanoparticles can be used as conductivity-reducing additives for polyolefin blends.

Conflicts of interest

There are no conflicts to declare.

Acknowledgements

We gratefully acknowledge the Swedish Foundation for Strategic Research (grant agreement FFL15-0147) for funding. We also thank the Chalmers Materials Analysis Laboratory (CMAL) for providing access to their LEO Ultra 55 SEM instrument.

References

1 T. Andrews, R. N. Hampton, A. Smedberg, D. Wald, V. Waschk and W. Weissenberg, *IEEE Electr. Insul. Mag.*, 2006, **22**, 5–16.
2 M. Mauri, A. I. Hofmann, D. Gómez-Heincke, S. Kumara, A. M. Pourrahimi, Y. Ouyang, P.-O. Hagstrand, T. Gkourmpis, X. Xu, O. Prieto and C. Müller, *Polym. Int.*, 2020, **69**, 404–412.
3 Y. Ouyang, A. M. Pourrahimi, A. Lund, X. Xu, T. Gkourmpis, P.-O. Hagstrand and C. Müller, *J. Polym. Sci.*, 2021, **59**, 1084–1094.
4 X. Huang, J. Zhang, P. Jiang and T. Tanaka, *IEEE Electr. Insul. Mag.*, 2020, **36**, 8–18.
5 S. Yu, S. H. Lee, J. A. Han, M. S. Ahn, H. Park, S. W. Han and D. H. Lee, *Polymer*, 2020, **202**, 122674.

6 X. Zhao, Y. Liu, J. Wu, J. Xiao, J. Hou, J. Gao and L. Zhong, *Global Energy Interconnection*, 2020, **3**, 120–127.
7 H. Ye, T. Fechner, X. Lei, Y. Luo, M. Zhou, Z. Han, H. Wang, Q. Zhuang, R. Xu and D. Li, *High Volt.*, 2018, **3**, 79–89.
8 G. Mazzanti and M. Marzinotto, *Extruded Cables For High–Voltage Direct–Current Transmission*, Wiley-IEEE Press, Hoboken, 2013, pp. 41–98.
9 A. S. Alghamdi and R. K. Desuqi, *Heliyon*, 2020, **6**, e03120.
10 M. G. Andersson, J. Hynynen, M. R. Andersson, V. Englund, P.-O. Hagstrand, T. Gkourmpis and C. Müller, *ACS Macro Lett.*, 2017, **6**, 78–82.
11 A. M. Pourrahimi, T. A. Hoang, D. Liu, L. K. H. Pallon, S. Gubanski, R. T. Olsson, U. W. Gedde and M. S. Hedenqvist, *Adv. Mater.*, 2016, **28**, 8651–8657.
12 B. Dang, J. Hu, Y. Zhou and J. He, *J. Phys. D: Appl. Phys.*, 2017, **50**, 455303.
13 A. M. Pourrahimi, S. Kumara, F. Palmieri, L. Yu, A. Lund, T. Hammarström, P.-O. Hagstrand, I. G. Scheblykin, D. Fabiani, X. Xu and C. Müller, *Adv. Mater.*, 2021, **33**, 2100714.
14 X. Chen, A. Paramane, H. Liu, J. Tie, Z. Wei and Y. Tanaka, *Polym. Eng. Sci.*, 2020, **60**, 717–731.
15 X. Chen, Z. Hong, C. Dai, M. Awais, F.-B. Meng, A. Paramane and H. Li, *J. Appl. Polym. Sci.*, 2022, **139**, e52314.
16 X. Chen, L. Yu, C. Dai, A. Paramane, H. Liu, Z. Wei and Y. Tanaka, *IEEE Trans. Dielectr. Electr. Insul.*, 2019, **26**, 2041–2049.
17 F. Nilsson, M. Karlsson, U. W. Gedde, R. Kádár, K. Gaska, C. Müller, P.-O. Hagstrand, R. T. Olsson, M. S. Hedenqvist and T. Gkourmpis, *Composites, Part B*, 2021, **204**, 108498.
18 T. Andritsch, A. Vaughan and G. C. Stevens, *IEEE Electr. Insul. Mag.*, 2017, **33**, 27–33.
19 S. Hu, Y. Zhou, C. Yuan, W. Wang, J. Hu, Q. Li and J. He, *High Volt.*, 2020, **5**, 249–255.
20 Y. Zhou, J. He, J. Hu and B. Dang, *J. Appl. Polym. Sci.*, 2016, 133.
21 Y. Zhou, J. Hu, B. Dang and J. He, *IEEE Trans. Dielectr. Electr. Insul.*, 2017, **24**, 1380–1389.
22 B. Dang, Q. Li, Y. Zhou, J. Hu and J. He, *Compos. Sci. Technol.*, 2017, **153**, 103–110.
23 E. Helal, C. Pottier, E. David, M. Fréchette and N. R. Demarquette, *Eur. Polym. J.*, 2018, **100**, 258–269.
24 S. Li, N. Zhao, Y. Nie, X. Wang, G. Chen and G. Teyssedre, *IEEE Trans. Dielectr. Electr. Insul.*, 2015, **22**, 92–100.
25 B. Nageshwar Rao and V. S. Nandakumar, *Mater. Today*, 2019, **18**, 994–1005.
26 J.-J. Park and J.-Y. Lee, *Mater. Chem. Phys.*, 2021, **270**, 124868.
27 Y. Zhou, C. Yuan, Q. Li, Q. Wang and J. He, *Glob. Energy interconnect.*, 2018, **1**, 520–526.
28 S.-J. Wang, J.-W. Zha, W.-K. Li, Y. Wang, Y.-Q. Wen, G. Chen and Z.-M. Dang, *Compos. Sci. Technol.*, 2016, **135**, 100–105.
29 D. Liu, A. T. Hoang, A. M. Pourrahimi, L. K. H. Pallon, F. Nilsson, S. M. Gubanski, R. T. Olsson, M. S. Hedenqvist and U. W. Gedde, *IEEE Trans. Dielectr. Electr. Insul.*, 2017, **24**, 1396–1404.
30 Y. Ouyang, A. M. Pourrahimi, I. Östergren, M. Mellqvist, J. Ånevall, A. Soroudi, A. Lund, X. Xu, T. Gkourmpis, P.-O. Hagstrand and C. Müller, *High Volt.*, 2022, **7**, 251–259.
31 D. Liu, A. M. Pourrahimi, R. T. Olsson, M. S. Hedenqvist and U. W. Gedde, *Eur. Polym. J.*, 2015, **66**, 67–77.
32 Y. Ouyang, M. Mauri, A. M. Pourrahimi, I. Östergren, A. Lund, T. Gkourmpis, O. Prieto, X. Xu, P.-O. Hagstrand and C. Müller, *ACS Appl. Polym. Mater.*, 2020, **2**, 2389–2396.
33 B. Fillon, A. Thierry, B. Lotz and J. C. Wittmann, *J. Therm. Anal.*, 1994, **42**, 721–731.
34 H. Bai, Y. Wang, L. Liu, J. Zhang and L. Han, *J. Polym. Sci., Part B: Polym. Phys.*, 2008, **46**, 1853–1867.
35 M. Blomenhofer, S. Ganzleben, D. Hanft, H.-W. Schmidt, M. Kristiansen, P. Smith, K. Stoll, D. Mäder and K. Hoffmann, *Macromolecules*, 2005, **38**, 3688–3695.
36 F. Nilsson, M. Karlsson, L. Pallon, M. Giacinti, R. T. Olsson, D. Venturi, U. W. Gedde and M. S. Hedenqvist, *Compos. Sci. Technol.*, 2017, **152**, 11–19.
37 F. Saiz and N. Quirke, *Phys. Chem. Chem. Phys.*, 2018, **20**, 27528–27538.
38 Y. Gao, B. Xu, X. Wang and T. Jia, *J. Phys. D: Appl. Phys.*, 2019, **52**, 285302.
39 A. T. Hoang, Y. V. Serdyuk and S. M. Gubanski, *Polymers*, 2016, 8.
40 F. Tian, Q. Lei, X. Wang and Y. Wang, *Appl. Phys. Lett.*, 2011, **99**, 142903.
41 M. Ji, D. Min, Q. Wu, W. Liu, S. Li, S. Qin and S. Zhu, *Composites, Part B*, 2022, **233**, 109649.
42 R. Borgani, L. K. H. Pallon, M. S. Hedenqvist, U. W. Gedde and D. B. Haviland, *Nano Lett.*, 2016, **16**, 5934–5937.
43 E. Kubyshkina, M. Unge and B. L. G. Jonsson, *J. Chem. Phys.*, 2017, **146**, 051101.